The Dual Gap Ionization Chamber: A novel Ionization Chamber design for reference dosimetry to automatically correct for recombination losses in emerging radiotherapy modalities.

Marina Orts[1], Séverine Rossomme[2], Kevin Souris[2], Victor de Beco[2], Thomas Haas[3], Norman Durny[3], Guillaume Houyoux[4], Sébastien Penninckx[4,5], Lies Verpoest[1], Verdi Vanreusel[6,7], Pierre Montay-Gruel[7,8], Peter Kuess[9,10], Hugo Palmans[9,11] and Edmond Sterpin[1,12,13].

[1] UCLouvain, Institut de Recherche Expérimentale et Clinique, Molecular Imaging Radiotherapy and Oncology (MIRO), Brussels, Belgium.
[2] Ion Beams Applications S.A., Louvain La Neuve, Belgium.
[3] Ion Beams Applications S.A., Dosimetry Business Unit, Schwarzenbruck, Germany.
[4] Radiophysics and MRI Physics Laboratory, Faculty of Medicine, Université Libre de Bruxelles, Brussels, Belgium.
[5] Department of Radiation Oncology, Institut Jules Bordet, Hopital Universitaire de Bruxelles (HUB), Université Libre de Bruxelles, Brussels, Belgium.
[6] Research in Dosimetric Applications, SCK CEN, Boeretang 200, 2400 Mol, Belgium.
[7] Antwerp Research in Radiation Oncology (AReRO), Centre for Oncological Research (CORE), University of Antwerp, Antwerp, Belgium.
[8] Radiation Oncology Department, Iridium Netwerk, Wilrijk, Antwerp, Belgium.
[9] MedAustron Ion Therapy Center, Wiener Neustadt, Austria.
[10] Division of Medical Physics, Department of Radiation Oncology, Medical University of Vienna, Vienna, Austria.
[11] National Physical Laboratory, Teddington, United Kingdom.
[12] KU Leuven, Department of Oncology, Laboratory of Experimental Radiotherapy, Leuven, Belgium.
[13] Particle Therapy Interuniversity Center Leuven, Particle, Leuven, Belgium.

Abstract

Objective: Current dosimetry protocols typically recommend multiple measurements to determine recombination correction factors (k_s), increasing the time required for dose measurements in the quality assurance workflow. We propose a novel dual-gap ionization chamber (DGIC) design for reference dosimetry featuring two air gaps of different thicknesses within a single device. This design enables the determination of k_s directly from the same measurements required to determine absorbed dose-to-water. Thus, eliminating the need for separate measurements to correct for recombination losses. The approach relies on analyzing the charge ratio between the two gaps, under Ultra High Dose Rates (UHDR) and dose per pulse (DPP) under Ultra High Dose per Pulse (UHDPP) conditions.

Approach: A DGIC prototype with electrode distances of 1 and 0.6 mm was developed and tested using different beam qualities: (1) a 240 MeV/u clinical carbon ion beam at conventional field dose rates of 25 Gy/min, (2) a 226 MeV continuous proton beam with a current between 5 and 800 nA at the cyclotron exit, where the maximum approximately corresponds to 200 Gy/s in the treatment room and (3) a 9 MeV electron beam with a DPP from 0.03 to 4.2 Gy, a frequency of 60 Hz and a pulse duration between 0.7 – 3.9 μs. k_s-factors were derived for the top cavity of 1 mm gap using the DGIC method and compared against the following: For proton and carbon ions, comparisons were made with the Jaffé plot method. For the electron beam, it was compared with a dose rate independent device, a flashDiamond detector, and the integrated current transformer of the LINAC.

Main results: A DGIC prototype was able to successfully correct for recombination losses under different beam modalities: for initial recombination in a clinical carbon ion beam, volume recombination in UHDR proton beam with field dose rates of 200 Gy/s and in UHDPP electron beams, where four pulses were delivered with DPP up to 4.2 Gy (this DPP corresponds to an effective pulse duration of 3.9 μs).

Significance: A DGIC design and its inherent method provides a practical and accurate way of determining dose and dose rate in emerging radiotherapy treatment modalities.

1. Introduction:

Air-filled Ionization Chambers (IC) are the gold standard for reference dosimetry in radiotherapy (RT) and are widely endorsed by international dosimetry protocols such as IAEA TRS-398 (INTERNATIONAL ATOMIC ENERGY AGENCY, 2024) and AAPM TG-51 (Almond et al., 1999). Their operation is based on measuring the charge generated by ionizing radiation within the air cavity, which is then corrected by various influencing factors and converted to absorbed dose-to-water using a calibration coefficient. One of these corrections is the ion recombination factor (k_s), which accounts for charge losses due to ion recombination prior to collection.

Ion recombination is typically categorized into initial recombination, occurring between charge carriers from a single ionizing particle track, and volume recombination, occurring between carriers from different tracks. Initial recombination depends on the Linear Energy Transfer (LET) of the incident radiation particle and is described by Jaffé's theory (Jaffé, 1913, 1929), while volume recombination is dose rate dependent and modeled by Boag's theories for both pulsed (Boag J W, 1950; J. W. Boag et al., 1996; J. W. Boag & Currant, 1980) and continuous beams (J. Boag & Wilson, 1952). However, it is important to note that these theoretical approaches exhibit limitations when extended to UHDR regimes.

Due to chamber-to-chamber variability and the sensitivity of theoretical models to physical parameters, generic or simulated k_s values cannot be confidently used, as they would introduce unreasonably large uncertainties. Instead, experimental determination for each specific IC under use is recommended (INTERNATIONAL ATOMIC ENERGY AGENCY, 2024). Among the different experimental methods to determine it, the two-voltage method (2VM), traditionally endorsed in TRS-398 for photon and electron beams, is the most widely used. However, its applicability becomes limited in emerging (high LET beams and UHDR/UHDPP) beam modalities.

In high-LET particle beams, typically used for their higher radiobiological effect, initial recombination is significant. As illustrative examples, (Rossomme et al., 2017) reported recombination losses of approximately 0.4% for a 115 MeV/u carbon ion beam, about 0.3% for a 50.57 MeV/u helium beam, and around 0.7% for a 103.77 MeV/u oxygen beam, measured in the plateau region with an Advanced Markus chamber operated at –300 V. Under these conditions, the 2VM is limited, as it should be used only if the inverse of the charge collected (1/M) is linear with the inverse of the applied voltage (1/V), a condition often unmet (INTERNATIONAL ATOMIC ENERGY AGENCY, 2024). Alternatives such as the three-voltage linear method (3VM) (Rossomme

et al., 2020) or the Jaffé plot method (now included in the revised version of the TRS-398), provide better accuracy but demand multiple measurements and corrections for charge multiplication for ICs with smaller air gaps (Rossomme et al., 2021).

Ultra High Dose Rates (UHDR) or Ultra High Dose Per Pulse (UHDPP) are beam delivery regimes required for FLASH radiotherapy. Due to the FLASH effect, consisting in the observation of a sparing effect on healthy tissue coupled to efficacious antitumor effect (Bourhis et al., 2019; M. Vozenin et al., 2024; M. Vozenin et al., 2022) compared to irradiation at conventional dose rate (∼Gy/min), FLASH-RT is of increasing interest in the radiotherapy field. In FLASH-RT, dose rates exceed conventional levels by several orders of magnitude (≳40 Gy/s) (Zhou et al., 2020). Under such conditions, recombination losses are substantial and compromise the validity of the 2VM.

Among the different accelerator options explored for UHDR proton beams, isochronous cyclotrons delivering quasi-continuous radiation have been investigated most extensively. In this case, volume recombination dominates and can be corrected if a linear behavior between 1/M and the inverse squared of the voltage ($1/V^2$) is observed (Lourenço et al., 2023). However, in the extreme case of UHDPP electron beams, recombination losses become even more pronounced, and all previous endorsed methods fail to determine k_s reliably.

Given these challenges, there has been significant interest in exploring other detector types. Despite advances, many alternatives such as alanine (Bourgouin et al., 2022), gafchromic films (Liu et al., 2023; Villoing et al., 2022), optically stimulated luminescence films (Motta et al., 2024), and inorganic or organic plastic films (Vanreusel et al., 2024) face limitations in real-time readout and some of them show limited dose rate dependency (Karsch et al., 2012). More promising developments include silicon carbide detectors (Fleta et al., 2024; Okpuwe et al., 2024; Paz et al., 2024) calorimeters (Bourgouin, Hackel, et al., 2023; Lourenço et al., 2023) and diamond-based detectors (Kranzer, Schüller, Bourgouin, et al., 2022).

Nevertheless, ICs are considered as a strong candidate for use in UHDR and UHDPP conditions since they are the gold standard in radiotherapy dosimetry. Recent research efforts on this class of detectors entail simulation-based studies (Christensen et al., 2020; Kranzer, Schüller, Rodríguez, et al., 2022; Paz-Martín et al., 2022), semi-analytical approaches (Bancheri & Seuntjens, 2024), extensions of theoretical models (Fenwick & Kumar, 2022), and experimental investigations of multiple ICs under UHDPP conditions (Bourgouin et al., 2023). Additional approaches focus on IC design improvements, such as using gases with low recombination rates (Martino et al., 2022), extremely reducing the air gap thickness (Gómez et al., 2022; Liu et al., 2024), or developing semi-empirical methods for correcting recombination in standard ICs (Petersson et al., 2017).

Overall, the main limitations of using conventional ICs under emerging modalities, particularly in UHDR conditions, are the complexity and labor-intensive nature of experimentally determining k_s for each specific chamber, as well as unresolved issues that persist in the highest dose per pulse (DPP) regions of the UHDPP regime.

In this work, we propose a novel IC design for reference dosimetry, the Dual Gap Ionization Chamber (DGIC), along with its inherent method (Prieels, 2009), already implemented in (Schaefer et al., 2023) with the dose monitoring ICs in the nozzle of a proton therapy system. This design integrates two ionization chambers within a single device, allowing for simultaneous reading of collected charges. By analyzing the variation in the charge ratio between the two gaps, the recombination correction factor k_s can be derived directly from the same measurements used to determine absorbed dose-to-water, thereby eliminating the need for separate measurements to account for recombination losses.

Since the method does not require any specific linear relationship between the inverse of the collected charge and inverse of the applied voltage, it is particularly suited for non-conventional conditions, including high-LET beams, UHDR and UHDPP. Furthermore, because the DGIC uses the response from both cavities, it can potentially provide additional information, such as real-time dose rate estimation through charge ratio variation, thus functioning as both for dose and dose rate determination.

2. Materials and methods:

2.1. Prototype design

The Dual Gap Ionization Chamber (DGIC) consists of two ICs with a different air gap size in face-to-face position separated by a thin layer of material within a single device. The DGIC prototype was designed according to the recommendations provided by TRS-398, which include: the use of near water-equivalent materials, a vented chamber design, a collecting electrode diameter not exceeding 20 mm, a cavity height not greater than 2 mm, and a guard ring width not smaller than 1.5 times the cavity height. Following those guidelines, a DGIC prototype was constructed (see Figure 1). To avoid damage and considering its potential use in UHDR conditions, the prototype was entirely made of polyether ether ketone (PEEK) and graphite (Orts et al., 2025). The 16 mm diameter collecting electrode is made of a thin layer of graphite of 25 μm. The guard ring has a width of 4 mm. The air gap thickness was set at 1 mm for the top cavity and 0.6 mm for the bottom cavity; further discussion on the selection of these air gaps is provided in Section 3.1.

Figure 1: External appearance of a DGIC prototype. The dimensions are comparable to those of a standard ionization chamber, though the chamber outer diameter is slightly larger (64 mm) to facilitate prototype assembly.

To limit potential dose gradients between both gaps, the piece of the ground electrode in the top chamber (0.5 mm thickness) also serves as part of the entrance window of the bottom chamber, as illustrated in Figure 2. Both gaps are electrically insulated from each other, with minimal influence of one into the other. Each gap functions as an independent ionization chamber and can be connected via triaxial cables to separate electrometers for simultaneous measurements.

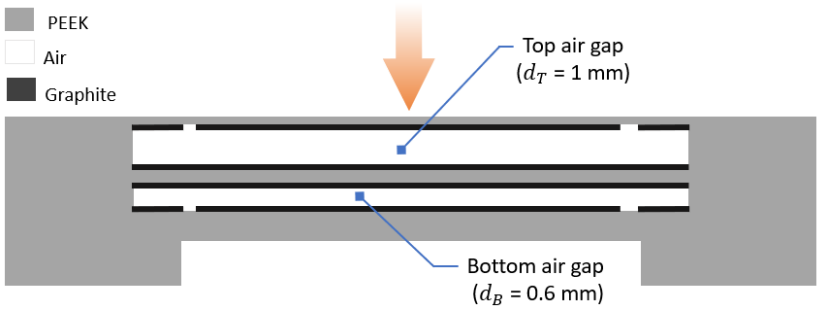

Figure 2: Schematic representation of the DGIC prototype geometry. The top air cavity has an electrode spacing of 1 mm (d_T), while the bottom cavity has a spacing of 0.6 mm (d_B). The two cavities are positioned face-to-face. The DGIC is irradiated from the top as indicated by the orange arrow.

2.2. Principle of use

The method used to determine the ion recombination correction factor is based on the semiempirical relation proposed by (Prieels, 2009):

$$\frac{1}{k_s^T} = 1 - \frac{1-\left(M_T/M_B\right)_N}{G} \qquad (1)$$

In this formulation, k_s^T is the ion recombination correction factor for the top gap, M_T and M_B are the charge reading in the top (T) and bottom (B) cavities, respectively. The ratio M_T/M_B is normalized by the ratio of their respective normalization factors, indicated by the subscript N, to account for differences in the signal between the two gaps. This normalization, adapted for reference dosimetry, is related to the ratio of their respective calibration coefficients (N_{D,w,Q_0}), which depends on the active volumes of the chambers and must include beam quality correction factors (k_{Q,Q_0}). The subscripts Q and Q_0 denote the user beam quality and the reference beam quality respectively. The normalized ratio is given by:

$$\left(M_T/M_B\right)_N = \frac{M_T/M_B}{N} = \frac{M_T/M_B}{\frac{N_{D,w,Q_0}^T}{N_{D,w,Q_0}^B}\frac{k_{Q,Q_0}^T}{k_{Q,Q_0}^B}} \qquad (2)$$

If the active volumes of both gaps have the same radius and no recombination losses are present, the signal amplification is ideally governed by the gap spacing ratio between the top (d_T) and

bottom (d_B) cavities (d_T/d_B), as noted by (Schaefer et al., 2023). However, due to manufacturing tolerances and assembly variability, the actual gap ratio may differ from the theoretical value. Although the calibration coefficients should ideally compensate for these differences, uncertainties in N_{D,w,Q_0} determination and the presence of charge multiplication in small gaps complicate this way of calibration. To improve accuracy, it is more reliable to determine the amplification coefficient N as the charge ratio corrected by charge multiplication, as described in (Rossomme et al., 2021), and subsequently applying a reliable method for correcting recombination losses in the calibration beam. Following TRS-398 recommendations, the use of the 2VM or Jaffé plot method in a Co-60 beam provides accurate results.

The parameter G in Equation (1) is a proportional factor obtained from a first-order Taylor series expansion of the specific recombination theories. It depends on the type of recombination, the gap spacing and applied voltage (this last quantity is denoted as V_T for the top cavity and V_B for the bottom cavity). When only initial recombination is present, or when the beam is considered pulsed (occurring when the pulse duration is shorter than the collection time of the IC and this collection time is shorter than the time between pulses (Palmans et al., 2006)), the expression for G is:

$$G_{pulsed/initial} = 1 - \frac{d_B^2/V_B}{d_T^2/V_T} \quad (3)$$

If the above conditions are not satisfied, the beam is considered as continuous or quasi-continuous (Palmans et al., 2006), and the corresponding expression for G is:

$$G_{cont} = 1 - \frac{d_B^4/V_B^2}{d_T^4/V_T^2} \quad (4)$$

Further information on the derivation of these expressions is provided in the supplementary materials. As a general guideline for identifying the applicable recombination regime for volume recombination: a beam may be considered pulsed when the pulse duration is much shorter than the ion collection time of the chamber and, in turn, this collection time is much shorter than the time between pulses. If any of these conditions is not fulfilled, the beam can be treated as continuous for the purpose of recombination modelling. We acknowledge that these criteria can become ambiguous in certain situations; therefore, in line with TRS-398 Rev.1 recommendations, we endorse performing experimentally at least once a full Jaffé plot characterization to verify the actual recombination behavior of the beam under study. In such plot, a linear relationship between the inverse of the charge collected (1/M) and inverse of the voltage (1/V) indicates behavior consistent with pulsed beams, whereas a linear dependence between 1/M and $1/V^2$ is characteristic of continuous beams. To further distinguish between initial and volume recombination, the dose rate may be varied: if the resulting Jaffé plot remains unchanged, initial recombination dominates, whereas changes in the Jaffé plot with dose rate indicate the dominance of volume recombination. This ensures consistent selection of the appropriate expressions for pulsed, continuous or initial recombination.

Note that N is a parameter that modulates the independent term of the calibration, whereas G modulates the slope. Once N and G are determined, Equation (1) allows the determination of k_s^T from a single simultaneous measurement of the charge collected in both gaps, which can be practically achieved simultaneously using two electrometers or a dual channel electrometer.

2.3. Modeling of the DGIC

Different calculations were performed to model the behavior of the DGIC under various conditions. These included understanding the operating principles of the method, optimizing air gap and voltage configurations, and determining relevant parameters such as the beam quality correction factors k_{Q,Q_0}.

A Monte Carlo based simulation tool was used to determine k_s in scenarios where analytical solutions to theoretical models are not found, which is the case for very low or very high k_s–values. The simulation models the distribution of charge carriers within the active volume of the ionization chamber, updating their positions in discrete time steps according to the relevant transport processes, followed by the Monte Carlo recombination algorithm proposed in (García et al., 2021). Initial recombination is modelled using a single ion track with a Gaussian radial charge distribution along the incident particle trajectory, while volume recombination is simulated by introducing multiple tracks according to the temporal structure of the beam. The ratio of initially generated to collected ions results in k_s. Further details on the implementation, intercomparison, and validation of this simulation tool can be found in (Orts et al., 2024).

To calculate the ratio of the beam quality correction factors as required for Equation (2), the beam quality correction factors k^i_{Q,Q_0} for each of the gaps (T: Top and B: Bottom) were calculated following the formalism described in (Andreo et al., 2013):

$$k^i_{Q,Q_0} = \frac{(D_w/\bar{D}_{air})_Q}{(D_w/\bar{D}_{air})_{Q_0}} \frac{w_{air,Q}}{w_{air,Q_0}} \quad \textit{with } i = T \textit{ or } B. \qquad (5)$$

where D_w denotes the local absorbed dose in water, $\bar{D}_{air}$ the averaged absorbed dose in the sensitive air volume of the IC and w_{air} the mean energy to create and ion pair in air. Following Equation (5), if the effective depth of measurement is the same for both cavities, then the ratio of the k_{Q,Q_0} factors between the top and bottom cavities is given by:

$$k^R_{Q,Q_0} \overset{\text{def}}{\equiv} \frac{k^T_{Q,Q_0}}{k^B_{Q,Q_0}} = \frac{(\bar{D}^T_{air}/\bar{D}^B_{air})_{Q_0}}{(\bar{D}^T_{air}/\bar{D}^B_{air})_Q} \qquad (6)$$

The Monte Carlo simulation toolkit Geant4-v11.2 (Agostinelli et al., 2003) was used to derive $\bar{D}_{air}$ values within the DGIC which was modelled using the material properties summarized in Table 1:

Material	I (eV)	$\rho\ (g/cm^3)$
Air	85.7	0.0012
Graphite	81.0	0.93
PEEK	74.1	1.31
Water	78.0	0.9982

Table 1: Material properties used for the simulation. Each material has its corresponding ionization potential (I) and density (ρ).

All the methodology on the Monte Carlo calculation of k_{Q,Q_0} factors is based on (Houyoux et al., 2025) including the different parameters presented in Table 2 as well as the physics list used for ^{60}Co photons and proton simulations. The physics list for protons was used for electrons, and also for carbon ions simulations for which the two following constructors were included: $G4RadioactiveDecayPhysics$ and $G4IonElasticPhysics$, following (Khan et al., 2021). For electrons, the beam parameters were based on the experimental conditions described below.

For each air cavity composing the DGIC, the corresponding reference point of measurement was defined at the inner center of the upper surface of the cavity. For the different particles, the positioning of the chamber was always accounting for the Water Equivalent Thickness (WET) of any non-water volume placed between the source and the cavity considered. Therefore, for top cavity simulations, the WET of the entrance window was considered, while for the bottom cavity simulations, the WET of the entrance window and the foil separating the two cavities were both considered.

Parameter	^{60}Co photons	Electron	Proton	Carbon
Beam shape	Square	Circle	Square	Square
Beam direction	Divergent	Parallel	Parallel	Parallel
Beam dimensions	10 x 10 cm^2	r = 4.5 cm	10 x 10 cm^2	10 x 10 cm^2
Beam energy	$(Mora\ et\ al., 1999)$	6, 9, 10, 12 MeV	226 MeV	240 MeV/n
Phantom size	20 x 20 x 20 cm^3	20 x 20 x 10 cm^3	20 x 20 x 10 cm^3	20 x 20 x 10 cm^3
Measurement depth	5 cm	1.5 g/cm^2	2 g/cm^2	1 g/cm^2
Cut Phantom	500 μm	500 μm	500 μm	500 μm
Cut Volume	1 μm	1 μm	1 μm	1 μm
dR/R – finalRange	0.003 – 1 nm	-	0.05 – 100 nm	-
Step limit	-	-	1 mm	-

Table 2: Summary of the simulation setups used for the Monte Carlo calculation of the k_Q factors. The symbol "-" characterizes the use of the default value for the parameter considered.

2.4. Experimental conditions

Experimental campaigns were performed at different centers to investigate the behavior of the DGIC in multiple conditions and beam qualities: (1) A Cobalt-60 source at the IBA Dosimetry Secondary Standard Laboratory (SSDL) in Schwarzenbruck, Germany; (2) a 240 MeV/u clinical carbon ion beam at the MedAustron Particle Therapy Center in Wiener Neustadt, Austria (Stock et al., 2018); (3) a 226 MeV quasi-continuous UHDR proton beam at the Fred Hutch Cancer Center in Seattle, USA; and (4) a 9 MeV UHDPP electron beam at the University of Antwerp, Belgium. For all experiments, both cavities of the DGIC were connected to two different Dose1 electrometers (IBA Dosimetry). Additionally, for the UHDPP experiment, two different DoseX electrometers (IBA Dosimetry) were used to investigate possible charge saturation caused by the Dose1 electrometers.

Beam	Center	Modality	Energy	Field	Ref. dosimeter
Cobalt-60	IBA SSDL	γ-ray source	~1.25 MeV	10 x 10 cm^2	PPC40
Carbon	MedAustron	Synchrotron	240 MeV/u	6 x 6 cm^2	PTW-34001
UHDR proton	Seattle	Isochronous cyclotron	226 MeV	8 x 8 cm^2	PPC05
UHDPP electron	Antwerp	LINAC	9 MeV	$\emptyset = 10\ cm$	flashDiamond

Table 3: Summary of the beams used to investigate the DGIC.

At the IBA Dosimetry SSDL, the DGIC prototype was calibrated with a Cobalt-60 source following TRS-398 procedures, with calibrations traceable to the Primary Standards Dosimetry Laboratory (PSDL) of PTB (Germany). The bias voltage over both gaps was set to -300 V during calibration. The top gap was calibrated at its reference depth; for the bottom cavity, the reference depth included the WET of the upper cavity and the thin separation layer between gaps. The Co-60 beam was also used to determine the charge multiplication correction factor (called k_{CM}) for each gap, since the small air gaps operated at high voltage makes this correction non-negligible. Following the method described by (Rossomme et al., 2021), Jaffé plots (1/M vs. 1/V) were obtained and fitted with a nonlinear least squares method on the exponential model:

$$k_s k_{CM} = \left(1 + \frac{A}{V} I_{sat}\right) e^{-\gamma \cdot V} \qquad (7)$$

where the first term (parameter A) corresponds to the initial recombination contribution (volume recombination was assumed to be negligible). The value of I_{sat} was estimated using a linear extrapolation of a linear fit from the Jaffé plot with data from $|1/V|$ = 0.01 – 0.05 V^{-1}. The second term, exponential with the voltage V, corresponds to the contribution of charge multiplication, where the parameter γ is a chamber-specific factor assuming to be independent of the beam quality according to (Rossomme et al., 2021) observations where the same charge multiplication correction factor was obtained in protons and a Cobalt-60 beam. This assumption is further supported by our measurements: when applying the derived k_{CM} in Co-60, the Jaffé plots followed the expected linear behavior (depending on the recombination regime) also at high voltages where charge multiplication is expected to affect the linearity, indicating consistent correction across different beam qualities.

At MedAustron, the DGIC was tested in a synchrotron-accelerated carbon ion beam to study initial recombination effects. A non-modulated Pencil Beam Scanning (PBS) field of 240 MeV/u (distal range R80 = 35 cm) was delivered in a 6 x 6 cm^2 field with 0.2 cm spot spacing. The DGIC prototype was positioned in a MP1 Manual MR Water Phantom (PTW-Dosimetry, Freiburg, (Germany)) at 1 cm depth in the plateau region according to TRS-398 Rev.1 recommendations for scanned beams, with a ROOS chamber – PTW 34001 (PTW-Dosimetry, Freiburg, (Germany)) placed behind the prototype under investigation to monitor beam fluctuations. To investigate potential contributions from volume recombination, a dose rate variation was introduced through three delivery settings: a 1 s spill duration, a 10 s spill duration, and a 10 s spill duration with a beam intensity reduced by 90%. These configurations corresponded to approximate field dose rates over the entire field delivery at the effective point of measurement of the IC of 25, 2.5 and 0.4 Gy/min, respectively. Note that the instantaneous dose rate experienced by the IC is substantially

higher and depends on the spot size, spacing, and scanning dynamics. Jaffé plots were obtained, corrected for k_{CM} previously obtained in Co-60, and fitted to the full Jaffé theory for initial recombination, following recommendations from (Rossomme et al., 2016), as traditional linear fits can lead to underestimations of experimental k_s-values. The free parameters N_0 and b from Jaffé's model (see Equation (A) in the supplementary material) were optimized and the resulting k_s^T-values were then compared with those obtained using the DGIC method.

At the Fred Hutch Cancer Center, the DGIC was studied under a quasi-continuous 226 MeV proton beam delivered by a cyclotron using an IBA Proteus Plus system. The beam was delivered in an 8 x 8 cm^2 scanned field composed of 100 spots of 7.5 mm (1 sigma). A wide range of beam currents at the cyclotron exit was used (8, 500 and 800 nA), with the highest setting corresponding to field dose rates at the measurement depth of approximately 200 Gy/s. Delivery times were extracted from the system log files, and the total dose was measured independently using an IBA PPC05 (IBA Dosimetry, Schwarzenbruck (Germany)) ionization chamber. Similarly to the carbon ion case, the instantaneous dose rate at the IC is considerably higher and depends on different parameters. Jaffé plots were obtained and corrected for k_{CM}. The resulting k_s^T-values obtained from the DGIC method were compared with those obtained using the Jaffé plot method.

At the University of Antwerp, the DGIC was tested in an UHDPP 9 MeV electron beam produced by an ElectronFLASH (EF) LINAC developed by S.I.T. (Italy). The beam was collimated with a 10 cm diameter applicator, with effective pulse durations ranging from 0.7 - 3.9 μs at a pulse frequency of 60 Hz. The number of pulses was fixed to 4, and the dose per pulse varied from 0.03 to 4.2 Gy. The source to surface distance (SSD) was set to 106 cm. The DGIC was positioned at 14 mm depth. A flashDiamond (fD) detector (PTW-Dosimetry, Freiburg, Germany)) was placed immediately after the DGIC. The Integrated Current Transformer (ICT) of the EF-LINAC was used to determine the number of pulses delivered. k_s^T was determined by fitting the experimental curves to Petterson's (Petersson et al., 2017) modified (Bourgouin et al., 2023) semiempirical equation:

$$k_s^{Petersson} = \left(1 + \left(\frac{DPP \cdot d^2}{V}\right)^{\alpha}\right)^{\beta} \qquad (8)$$

Where DPP is the Dose per Pulse in mGy, d the air gap size in mm, V the bias voltage in V, and α and β fitting parameters. The resulting k_s^T were then compared to the value obtained using the DGIC inherent method.

3. Results:

3.1. Simulations, calibration and calculations on the DGIC design

Figure 3 (a) shows the variation of the parameter G from Equation (1), for different recombination regimes (initial, volume pulsed and continuous) as a function of the air gap ratio d_B/d_T, for various voltage ratio configurations V_T/V_B between the top (T) and bottom (B) cavities.

A higher G-factor is preferable, as it enhances the charge difference between the two ionization chambers, thereby improving the method's accuracy by increasing its sensitivity. As shown, G

increases when the gap ratio d_B/d_T decreases or when the voltage ratio V_T/V_B is increased. However, reaching G-factor values close to 1 can be practically challenging: Small d_B/d_T ratios require large disparity in the absolute gap sizes, necessitating either very large or very small gaps. Large gaps are unsuitable for UHDR applications, as they lead to excessive recombination effects, and given that, it would surpass the TRS-398 recommendation of 2 mm. Conversely, very small gaps are challenging to manufacture, can compromise the fabrication reliability and lead to larger multiplication effects. Similarly, while increasing V_T/V_B enhances G, similar issues occur: low bias voltages in one gap can result in significant recombination, while excessive high voltages may induce significant charge multiplication effects, which deviate from ideal ionization chamber behavior.

A balanced and practical configuration, which does not deviate much from already existing traditional ICs designs, is achieved by setting the top and bottom gaps to 1 and 0.6 mm, respectively, with an equal bias voltage of -300 V. This corresponds to a theoretical gap ratio d_B/d_T = 0.6 and a voltage ratio V_T/V_B = 1, which results in theoretical gains of $G_{cont} = 0.87$ and $G_{pulsed/ini} = 0.64$.

Figure 3 (b) shows the theoretical variation of the charge collection efficiencies (f, inverse of k_s) for a continuous proton beam with the chosen configuration for the DGIC prototype (d_T = *1 mm*, d_B = *0.6 mm*, V_T = *-300 V and* V_B = *-300 V*) as well as the components of Equation (1) versus the dose rate. The G factor remains constant across a large dose rate range, showing the feasibility of using this method even at UHDR.

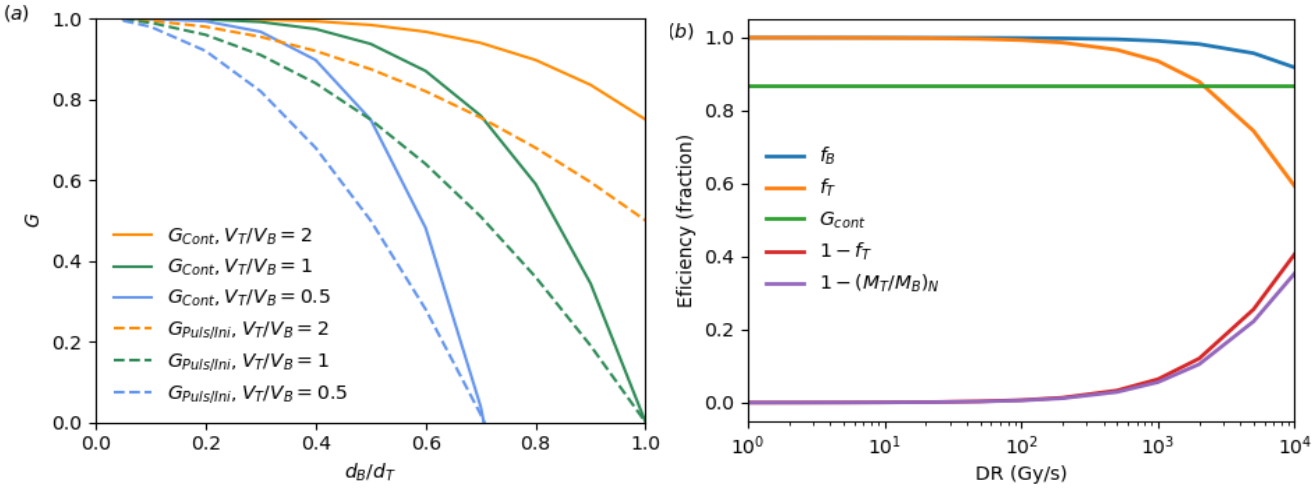

Figure 3: (a) Theoretical dependence of the G-values on the theoretical gap ratio d_B/d_T for volume recombination in quasi-continuous beam (continuous lines) and pulsed beams or initial recombination (dashed lines) for different voltage ratios between the top and bottom cavities V_T/V_B. (b) Theoretical variation of the efficiency in a continuous proton beam of the top gap (orange line), the efficiency of the bottom gap (blue line), the nominator (purple line) of Equation (1), denominator (red line) of Equation (1), and G_{cont} (green line) of Equation (1) as a function of the dose rate (DR) for the specifications of the DGIC prototype developed in the present study.

The DGIC was successfully calibrated in a Co-60 beam, with absorbed dose to water calibration coefficients for each gap of $N_{D,w,Q_0}^{T} = 0.1424\ Gy/nC$ and $N_{D,w,Q_0}^{B} = 0.2197\ Gy/nC$ (standard uncertainty of 1.1%, coverage factor k=1).

For the method calibration, the relative type-A uncertainty, estimated from the standard deviation of the mean of the measured current was lower than 0.1%. The gamma parameter of Equation (7) obtained for the top and bottom cavity were $\gamma_T = (2.13 \pm 0.16) \cdot 10^{-5}\ V^{-1}$ and $\gamma_B = (3.54 \pm 0.21) \cdot 10^{-5}\ V^{-1}$, respectively. As expected, the smaller gap, (i.e. bottom cavity) yielded higher charge multiplication, and the larger gap (i.e. top cavity), smaller. At the calibration voltage of -300 V this resulted in a charge multiplication correction of about 0.6% for the top cavity and a 1.1% for the bottom cavity. This k_{CM} correction factors are applied throughout the entire study, assuming beam quality independency, in cases where the DGIC is used in a different bias voltage as the one it was calibrated.

At the bias voltage of -300V, the measured charge ratio $M_T/M_B = 1.562$ was corrected by $\frac{k_s^T}{k_s^B} \cdot \frac{k_{CM}^T}{k_{CM}^B}$ = 1.004 which results in an experimental normalization value of N = 1.568 $\propto \frac{d_T}{d_B}$. Accordingly, the experimentally determined G-factors were $G_{cont}^{exp} = 0.835$ and $G_{pulsed/ini}^{exp} = 0.593$. This differences between theoretical and experimental values are attributed to the differences in manufacturing tolerances in the air gap size (up to +0.05 mm larger than the nominal value), and lie within the expected ranges: $G_{cont}^{exp} = 0.821 - 0.893$ or $G_{pulsed/ini}^{exp} = 0.578 - 0.673$. These deviations from expected values show the importance of determining these factors experimentally.

As the DGIC was tested in different beam qualities: electron, proton and carbon ion beams, Monte Carlo simulations were carried out to determine the beam quality correction factor of each of the gaps, to determine the ratio as needed for Equation (2). The values of k_{Q,Q_0}^{R} for the different beam qualities are presented in Table 4. All values, regardless of the particle beam type, agree with each other and with unity within the 1σ level. Consequently, in the following analysis, $k_{Q,Q_0}^{R} = 1$ is adopted as a reasonable assumption.

Particle	*Energy (MeV)*	k_{Q,Q_0}^{R}
Electron	*6*	*1.000(6)*
	9	*1.002(6)*
	10	*1.003(6)*
	12	*1.000(6)*
Proton	*226*	*1.004(6)*
Carbon	*240 / n*	*1.001(6)*

Table 4: Numerical k_{Q,Q_0}^{R} values for electrons, protons and carbon ions in this study. The values with parenthesis correspond to one standard deviation of the last digit.

3.2. Correction for initial recombination

Figure 4 (a) shows the Jaffé plots measured for the top cavity of the DGIC prototype in a 240 MeV/u carbon ion beam at the three different dose rates investigated. The relative type-A uncertainty of the measured current was 0.1% or smaller for the bias voltage of -300 V and increases for lower voltages which explain the differences observed between the Jaffé plots for different dose rates. A Monte Carlo calculation for k_s determination with the simulation tool described in section 2.3 were conducted for the three different dose rates, assuming an IC with a 1mm air gap operated at -300 V and using the specific b and N_0 parameters from Jaffé's model obtained below for this beam. As shown in table 5, there is a minimal contribution of volume recombination, between 0.4 – 1.8 % of the total recombination. This confirms that the differences observed are due to experimental variability, and that only initial recombination is present.

	0.4 Gy/min			25 Gy/min		
Voltage (V)	*Total k_s*	*% Initial*	% Volume	*Total k_s*	*% Initial*	% Volume
300	*1.006(1)*	*99.6*	*0.4*	*1.006(1)*	*99.6*	*0.4*
100	*1.017(2)*	*99.5*	*0.5*	*1.017(2)*	*99.5*	*0.5*
50	*1.031(3)*	*99.5*	*0.5*	*1.031(3)*	*99.5*	*0.5*
20	*1.068(4)*	*99.4*	*0.6*	*1.069(3)*	*98.2*	*1.8*

Table 5: Theoretical calculations with the Monte Carlo simulation for k_s determination of the contribution of initial and general recombination in the top gap of 1 mm for the smallest and largest dose rates investigated in the 240 MeV/u carbon ion beam, for different voltages. The calculations show a negligible contribution of the volume recombination.

Figure 4 (b) shows the variation of k_s^T with |1/V| for the different methods: Jaffé's model, Jaffé plot method and DGIC method. Fit to the Jaffé's theoretical model parameters, the values found were: $N_0 = 91899 \pm 4225$ ion pairs/cm and b = 0.0045 $\pm$ 0.0014 cm from Equation (A) in Appendix 6.1., in line with expected values (Rossomme et al., 2016). To obtain k_s^T through the DGIC method, N-value and G_{ini}-experimental values for the initial recombination were applied, obtained from previous calibration in Co-60. No k_{Q,Q_0}^R correction was applied as previously explained. There is good agreement between the different methods, with maximum relative differences of 0.5% across the whole voltage range.

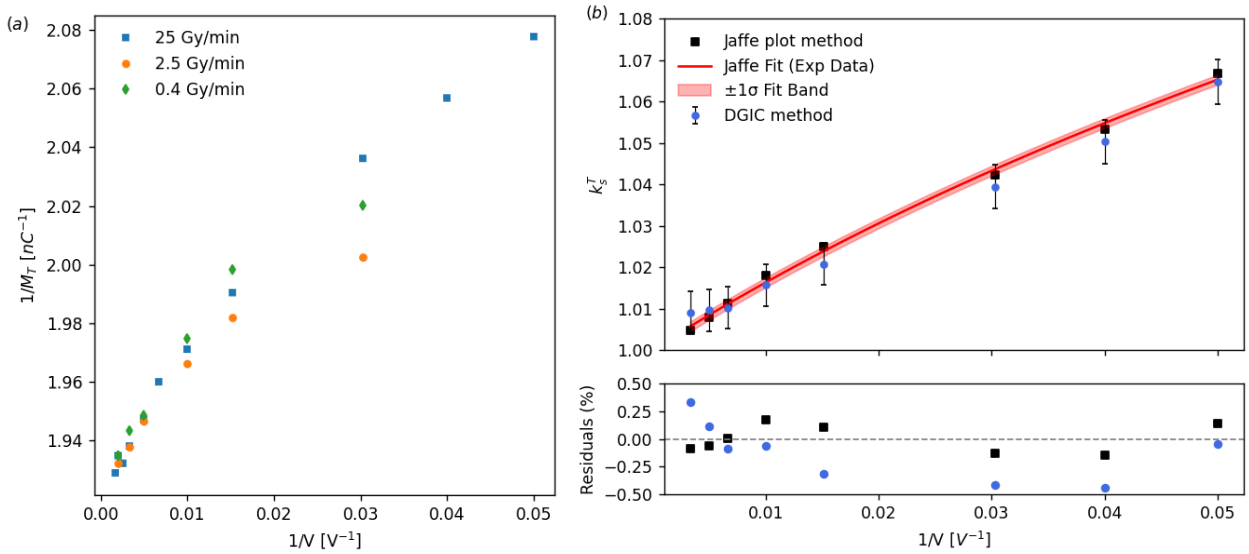

Figure 4: (a) Jaffé plots from the top cavity for the various dose rates investigated across different experimental campaigns. (b) Variation with |1/V| of Jaffé plot method (black points), k_s^T-values obtained by fitting to Jaffé theory (red line) including the 1σ confidence band, and k_s^T-values determined with the DGIC method (blue dots).

3.3. Correction for volume recombination

3.3.1. Protons UHDR, continuous beams

To determine k_s^T using the DGIC method in a 226 MeV proton beam, experimental values for the N-value and G-value (specifically G_{cont}, as volume recombination in a quasi-continuous beam is studied) were applied. As in the previous section, k_{Q,Q_0}^R- value was taken as 1. The relative type A uncertainty of the measured current was around 0.1% for the lower voltage ranges (-500 to -100 V). For smaller voltage ranges, the standard deviation of the averaged measured current was between 0.2 and 0.4%.

Figure 5 shows the variation of k_s^T with |1/V|, calculated using both the DGIC method and the Jaffé plot method. As expected in a quasi-continuous beam where volume recombination dominates, a quadratic trend of k_s versus |1/V| is observed. At the lowest dose rate (i.e. 5 nA), in conventional mode, small recombination losses (below 1% at the bias voltage of -300 V) are present. As the dose rate increases, k_s^T also increases up to 1.6% (at the bias voltage of -300 V), indicating the expected dose-rate dependence of k_s. The agreement between the two methods at -300 V (residuals at |1/V| = 0.0033 V^{-1} in Figure 5) is within 0.5% across all three dose rates. For smaller bias voltages (larger 1/V values in Figure 5), the agreement between the methods differs, which may be attributed to the larger uncertainties associated at lower voltages as discussed in Appendix 6.4.

Following the recommendations of (Bourgouin et al., 2023), which suggest a potential dependence of charge collection efficiency on temperature and atmospheric pressure due to changes in ion mobility, environmental conditions were carefully monitored. During this

experimental campaign, temperatures ranged from 20.5 °C to 21.4 °C, and atmospheric pressures ranged from 999.4 hPa to 1000.4 hPa. All charge measured when applying the Jaffé plot method was corrected using the temperature–pressure correction factor ($k_{T,P}$) endorsed in TRS-398. For the DGIC method, both charge readings are equally affected by $k_{T,P}$. As this correction factor is independent on the chamber geometry the ratio between the two cancel out, making this correction on each measurement unnecessary.

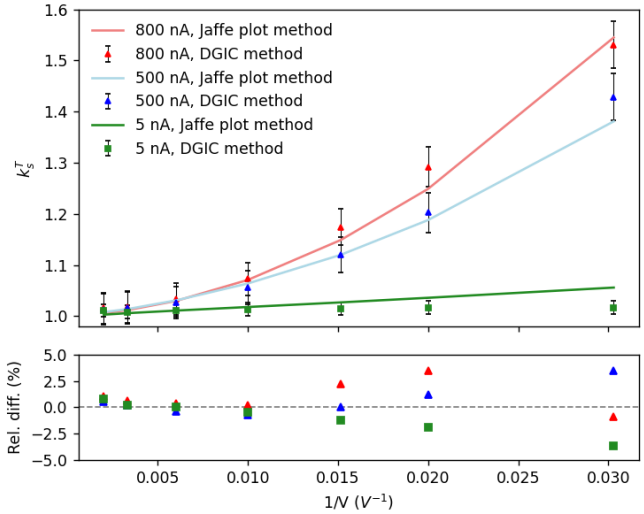

Figure 5: Variation of k_s^T with |1/V| for the three dose rates investigated: 800 nA (corresponding to about 200 Gy/s, shown in red), 500 nA (corresponding to about 130 Gy/s, (blue) and 5 nA (conventional dose rate, corresponding to about 15 Gy/min, in green). Values were obtained using the Jaffé plot method (solid lines) and the DGIC method (scattered points).

3.3.2. Electrons UHDPP, pulsed beams

k_s^T was determined with the DGIC method following the procedure in Sections 3.2 and 3.3.1, but using G_{pulsed} as this part addresses the case of volume recombination in a pulsed beam. The fD DPP values are shifted to lower values relative to those obtained with the DGIC, since the fD was positioned after the DGIC prototype, in the region of the PDD curve where the dose decreases with depth. To enable comparison of DPP values beyond the range measured with the fD, its response curve was extrapolated, given that its response is linear with dose. The relative type-A uncertainty in the measured current was around 1% for the fD and approximately 0.6% for the DGIC prototype.

Figure 6 (a) shows the dose determined in the 9 MeV UHDPP electron beam with the DGIC as a function of the DPP obtained with two DoseX electrometers, comparing results obtained without correction for recombination losses, with those corrected using k_s^T, and with the dose measured with the flashDiamond (fD). Not correcting for recombination can lead to a significant underestimation of dose (up to 90% at DPP values around 4.2 Gy). Applying the DGIC method to correct for recombination enables improved dose determination.

Figure 6 (b) shows the same plot if two Dose1 electrometers are used, where the response of the DGIC saturates around 1.2 Gy as the instantaneous current produced by the radiation pulse exceeds the maximum current supported by the electrometer (Gómez et al., 2022). This behavior is linked to the internal architecture of the DOSE-1: it relies on charge–discharge cycles of an internal capacitor, which can saturate when exposed to high instantaneous pulse currents. In contrast, the DOSE-X employs an integration method better suited for pulsed beams and does not show this limitation within its specified operating range (24–65 nC per pulse at repetition frequency of ≤400 Hz or 400 fA–24 μA in current).

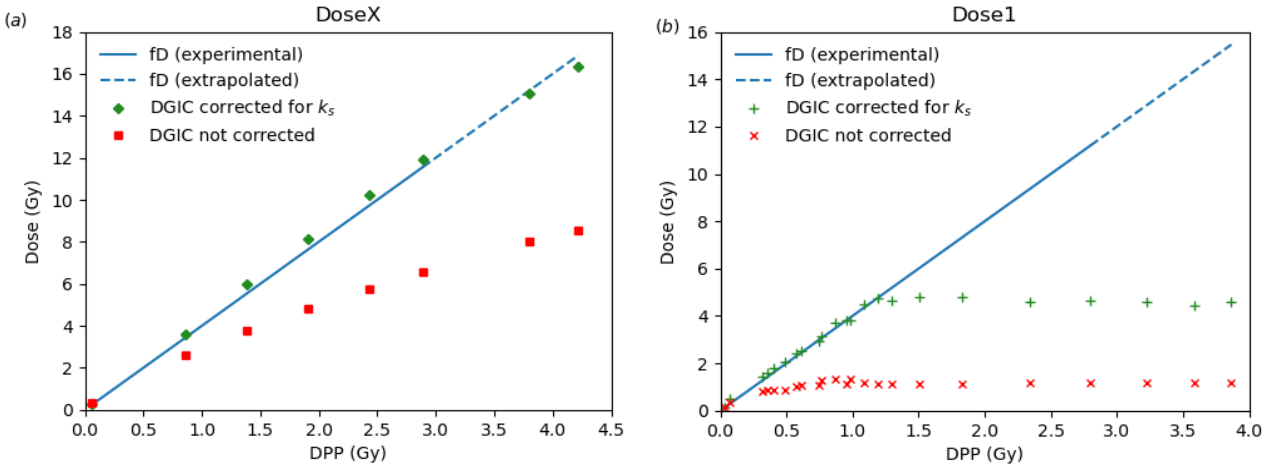

Figure 6: (a) Dose versus DPP obtained experimentally with the flashDiamond (fD, solid blue line), extrapolated values (fD, dashed blue line), DGIC corrected for recombination losses (green diamonds) with the DGIC method, and DGIC not corrected for k_s (red squares) obtained with two DoseX electrometers. (b) Similar graph but obtained with two Dose1 electrometers where in this case the green crosses represent the DGIC corrected for recombination losses with the DGIC method and the red plus symbol represent the uncorrected values.

Figure 7 shows k_s^T obtained with the DGIC method and compared with the Petersson semiempirical model (Equation (8)), with fitting parameters found to be α=0.83 and β=0.35, consistent with values reported in the literature (Bourgouin et al., 2023; Petersson et al., 2017).

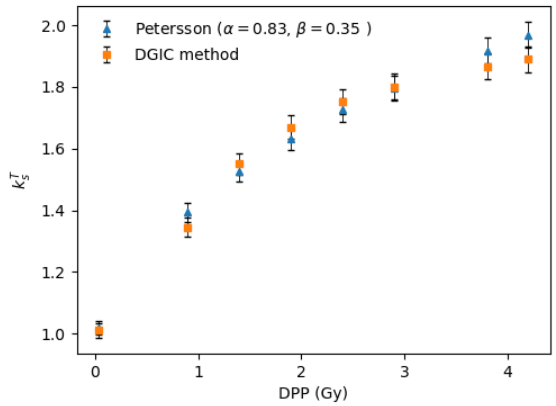

Figure 7: k_s^T-values determined with the Petersson semiempirical model (blue triangles) compared with the DGIC method (orange squares) and its corresponding uncertainties in k_s determination.

Although larger DPP values have not been explored in this work to address limitations of the method, we do not recommend operating the DGIC at such high DPP conditions, as the recombination correction factor becomes impractically large (e.g., k_s^T ≈1.9 at 4.2 Gy per pulse), leading to unacceptable uncertainties in the total dose estimation.

4. Discussion:

The DGIC method presents a novel and practical approach to correct for ion recombination in ionization chamber thanks to its unique double air gap design within the same device. By measuring the ratio of collected charges in each gap at their respective bias voltage, the method enables the determination of the recombination correction factor k_s for one of the gaps in a single measurement, in contrast with other commonly used methods. While the 2VM remains the standard recommended in TRS-398, the updated guidelines acknowledge the need for more accurate alternatives, particularly in particle beams where the dominance of initial recombination and/or the presence of charge multiplication distorts the linearity requirement needed to apply the 2VM. Methods such as the Jaffé plot method, while more accurate, require multiple measurements with varying voltages, associated with longer stabilization times of the IC, making them less practical for routine clinical use.

The DGIC method can be easily calibrated by directly evaluating the charge ratio, ideally without recombination losses in a Cobalt-60 beam, while accounting for charge multiplication and any minimal recombination present using the procedures described in Section 2.2. This approach makes the DGIC method adaptable to a wide range of conditions, capable of correcting both initial and volume recombination, covering UHDR conditions and, to a limited extent, UHDPP.

For UHDPP electron beams, where the achieved DPP are highest, the DGIC method has shown to work for the full range of DPP covered in this study. Initially, measurements beyond 1.2 Gy per pulse with Dose1 electrometers appeared unreliable, suggesting a possible breakdown due to either saturation of the electrometers or space-charge screening effects that distort the effective

electric field and violate the assumption of a constant G-value. The latter explanation, however, would be expected to produce a more gradual failure of the method. Repeating the experiment with more suitable electrometers (DoseX) confirmed that the method itself remains valid, and that the apparent deviation was caused by limitations of the Dose1 electrometer. This highlights the critical importance of using equipment compatible with UHDPP conditions, as inadequate instrumentation can lead to erroneous characterization of detector response and misleading conclusions about the underlying physical behavior. As an alternative mitigation strategy for this saturation effect, (Gómez et al., 2022) proposed placing an external capacitor in parallel with the signal cable to reduce the peak voltage at the electrometer input (e.g., by connecting an nF-range capacitor between the collection electrode and the guard of the triaxial cable). Such approach may help prevent saturation in electrometers with limited instantaneous current handling capability.

Larger DPP values that would allow a deeper exploration of the method's limitations due to space charge screening have not been investigated in this work. Nevertheless, our findings already indicate that operating the DGIC at very high DPP conditions is not advisable (e.g., 52% correction to the measured charge at 4.2 Gy per pulse), as the required recombination correction factor becomes impractically large and would result in unacceptable uncertainties in the estimated dose.

Reducing the air gap could extend the operational range, as explored in other studies (Gómez et al., 2022; Liu et al., 2024). However, such extreme designs would likely increase charge multiplication (Rossomme et al., 2021) and present challenges in manufacturing a DGIC with high precision.

Appendix 6.4 details the main sources of uncertainty considered in this work. For the conditions studied here, the total uncertainty in k_s with the DGIC method is estimated to be 0.62% for carbon ions (k_s∼1.01), 0.85% for the UHDR proton beam (k_s∼1.015), and 2.36% for the UHDPP electron beam (k_s∼1.5). When compared with other methods, (Rossomme et al., 2016) reported a combined relative standard uncertainty for k_s on carbon ion beams of 0.36% using the Jaffé plot method. For UHDR proton beams, (Lourenço et al., 2023) estimated the uncertainty of the Jaffé plot method to be 0.2%; however, this estimate was addressed only under conventional dose rates and is therefore likely underestimated in the UHDR regime (Lourenço et al., 2023). For UHDPP electron beams, the reported uncertainties vary depending on the method: dose comparison with water calorimetry yields an uncertainty of about 1.3% (Bourgouin, Hackel, et al., 2023), while the Petersson semi-empirical model (for a specific chamber) indicates an uncertainty of 2.2% (Petersson et al., 2017). From this comparison, the DGIC method results in larger uncertainties in some cases. However, an important advantage is that it does not require additional measurements to determine k_s. As described in Appendix 6.4, the total uncertainty of the method is mainly influenced by the uncertainty in the measured current and the calibration of the detector. A promising way to significantly reduce this uncertainty would be to calibrate the device against a primary standard, such as a calorimeter, at the beam quality of interest. This

approach may offer a practical compromise between time in clinical workflow efficiency and accuracy.

5. Conclusion:

This work presents and validates a new method for correcting ion recombination based on a dual-gap ionization chamber design tailored for reference dosimetry. The method enables accurate determination of k_s in the top cavity from a single measurement, by exploiting the relationship between the collected charge between the two gaps. It has been demonstrated to be effective to correct for initial recombination in a carbon ion beam, a continuous UHDR proton beam, and, within a limited range, under a UHDPP electron beam, offering a practical solution where conventional methods are less feasible to use due to the requirement of performing multiple measurements to assess k_s.

The DGIC method has been tested and remains valid to use up to 4.2 Gy per pulse, the limit of this study. Furthermore, while not yet explored in this study, the DGIC may be particularly well suited to UHDPP proton beams, where DPP values are generally lower than in electron beams. This represents a promising direction for future research.

Beyond recombination correction, the DGIC has the potential to provide dose rate estimates, taking advantage of its ability to simultaneously measure the charge collected in both gaps as noted in (Prieels, 2009). In pulsed beams, it could be used to determine the instantaneous dose rate or the dose per pulse, while in continuous beams, it would allow the measurement of the average dose rate. The underlying principle would be similar to that used for the determination of k_s^T: the ratio of charges measured in the two gaps must be first normalized, as previously described in the main method, and then related to the dose rate using a calibration-derived conversion factor. The dose rate measured by the DGIC would then be given by:

$$DR_{DGIC} = \frac{\left(\frac{M_T}{M_B}\right)_{norm}^{-1}}{CF} \qquad (9)$$

Where CF is a conversion factor that converts the normalized charge ratio to dose rate (DR). To determine CF for a given beam, the same expression is used but with the dose rate obtained from an independent method. However, this approach is only valid if a linear relationship between the recombination correction factor and the dose rate is observed. Once calibrated, the DGIC would offer a practical, real-time method to determine the dose rate in UHDR conditions, offering added value for quality assurance in UHDR, where independent dose rate verification would be required.

The theoretical basis of the DGIC method also suggests potential for estimating LET, in a manner analogous to the dose rate estimation. This has been explored in liquid ionization chambers (Rodríguez et al., 2012; Tegami et al., 2017), but could not be achieved with the present geometrical configuration due to the small air gaps used in the current design, optimized to minimize recombination in UHDR conditions. Previous work by (Rossomme et al., 2016) demonstrated that LET effects on k_s become detectable with larger air. For example, with a 2 mm

gap operated at –100 V, differences of approximately 5% were observed between the plateau region and the Bragg peak; this sensitivity increased to around 15% when the voltage was further reduced to –33 V). The underlying concept could be adapted to other devices, such as large-area ionization chambers used in hadron therapy (Kuess et al., 2017; Osorio et al., 2021). In such applications, the same dual-gap principle could be used to simultaneously assess dose and LET through depth dose curve measurements. This possibility, though not addressed experimentally in this study, offers an interesting direction for future work.

The DGIC method provides a practical alternative to conventional recombination correction techniques with ionization chambers. By enabling the determination of k_s from a single measurement, it reduces the complexity of deriving recombination losses and eliminates the need for multiple voltage acquisitions. The method's feasibility, along with its conceptual and experimental validation under the different conditions explored in this study, provides a solid basis for continued development and refinement.

6. Appendix:

6.1. Derivation of G factor for initial recombination

Jaffé theory for initial recombination (Jaffé, 1913, 1929) states that the efficiency of a plane parallel IC- i with d_i distance between plates (cm) due to initial recombination losses when the incident radiation particle is parallel to the electric field is:

$$f_i^{ini} = \frac{e^{-1/g}}{g q_i}\left[li\left(e^{\frac{1}{g}+ln(1+q_i)}\right) - li(e^{1/g})\right] \text{ with } q_i = \frac{2d_i^2 D}{\mu b^2 V_i} \text{ and } g = \frac{\alpha N_0}{8\pi D} \qquad \text{(A)}$$

Where li is the logarithmic integral, D is the diffusion constant of ions $(cm^2/V \cdot s)$, μ is the mobility of ions or ion drift coefficient $(cm^2/V \cdot s)$, b is the gaussian radius (cm), V_i is the bias voltage of IC-i (V), α is the recombination constant (cm^3/s) and N_0 is the linear charge carrier density $(ions/cm)$.

If a first order Taylor series expansion is performed around $q_i = 0$, i.e., considering near saturation condition, the previous equation becomes:

$$f_i^{ini} \approx \frac{1}{1+C_{ini}\frac{d_i^2}{V_i}} \text{ where } C_{ini}=\frac{gD}{\mu b^2} \qquad \text{(B)}$$

If $f = 1/k_s$, substituting M_T and M_B using the TRS-398 equation for reference dosimetry:

$$D_{w,Q} = \left(M_Q\, k_{TP} k_s k_{pol}\right) N_{D,w,Q_0} k_{Q,Q_0} \qquad \text{(C)}$$

and assuming no dose gradients are present and that the dose measured in both gaps is the same, if $k_{TP}^T = k_{TP}^B$, $k_{pol}^i = 1$, Equation (1), Becomes:

$$G = \frac{1-\left(f_T/f_B\right)}{1-f_T} \qquad (D)$$

Substituting (B) into (D), simplifies all dependencies on different parameters included in C_{ini}, allowing us to obtain G for initial recombination:

$$G_{ini} = 1 - \frac{d_B^2/V_B}{d_T^2/V_T} \qquad \text{(E)}$$

6.2. Derivation of G factor for volume recombination, pulsed beams

(Boag J W, 1950) found that the collection efficiency when volume recombination of a plane parallel IC-i is present in a pulsed beam is:

$$f_i^{pulsed} = \frac{1}{u_i}\ln(1+u_i) \text{ with } u_i = \frac{2\alpha d_i^2 \bar{q}}{e\mu V_i} \qquad \text{(F)}$$

Where $\bar{q}$ is the charge density (C/cm^3) and e is the electronic charge (C).

If a Taylor series expansion is performed around $u_i = 0$, the previous equation becomes:

$$f_i^{pulsed} \approx \frac{1}{1+C_{puls}\frac{d_i^2}{V_i}} \text{ where } C_{pulsed}=\frac{\alpha\bar{q}}{e\mu} \qquad (H)$$

Similarly as in previous section, substituting (H) into (D) allows us to determine G for pulsed beams, which is the same expression as obtained for initial recombination:

$$G_{pulsed} = 1 - \frac{d_B^2/V_B}{d_T^2/V_T} \qquad \text{(I)}$$

6.3. Derivation of G factor for volume recombination, continuous beams

Similarly, for a continuous beam (J. Boag & Wilson, 1952):

$$f_i^{cont} = \frac{2}{1+\sqrt{1+\frac{2}{3}\delta_i^2}} \text{ with } \delta_i^2 = \frac{\alpha d_i^4 \bar{\bar{q}}}{e\mu^2 V_i^2} \qquad \text{(J)}$$

Where $\bar{\bar{q}}$ is the ionization intensity ($C/cm^3 \cdot s$).

if a Taylor series expansion is performed around $\delta_i = 0$, the previous equation becomes:

$$f_i^{cont} \approx \frac{1}{1+C_{cont}\cdot\frac{d_i^4}{V_i^2}} \text{ where } C_{cont}=\frac{\alpha\bar{q}}{e\mu^2} \qquad (K)$$

Substituting (K) into (D) allows us to determine G for continuous beams:

$$G_{cont} = 1 - \frac{d_B^4/V_B^2}{d_T^4/V_T^2} \qquad \text{(L)}$$

6.4. Uncertainty on the DGIC method

All quoted uncertainties in this work are expressed as a standard uncertainty (k=1). The uncertainty associated with the DGIC inherent method was evaluated from the contributions from different parameters to the overall uncertainty on k_s, which arise from the following sources:

Bias voltage: The electrometers used in this work provided highly stable bias voltage for each of the gaps (V_i, with i=T,B). With an estimated uncertainty in each voltage (u_{V_i}) of 1 V (type B) and a nominal bias of -300 V for both gaps, the relative uncertainty in the bias voltage ratio (u_{V_R}), obtained using Gaussian error propagation: $u_{V_R}^2 = \left(\frac{\partial V_R}{\partial V_T}\right)^2 u_{V_T}^2 + \left(\frac{\partial V_R}{\partial V_B}\right)^2 u_{V_B}^2$, is approximately 0.001%. At lower voltages the relative contribution is larger (e.g., 0.16% at 30 V).

Air gap thickness: According to the methodology presented in earlier sections, the air-gap ratio can be obtained from the N_{D,w,Q_0}^i ratio of each of the gaps (i=T,B): $\frac{d_T}{d_B} = \frac{N_{D,w,Q_0}^T}{N_{D,w,Q_0}^B}\frac{k_{Q,Q_0}^T}{k_{Q,Q_0}^B}$. However, because the uncertainty in each N_{D,w,Q_0}^i is typically 1.1%, the propagated uncertainty in the gap size ratio becomes unreasonably large. The alternative method described in section 2.2. is therefore used, where the air gap size ratio can be obtained from: $\frac{d_T}{d_B} = \frac{M_T}{M_B}\frac{k_s^T \cdot k_{CM}^T}{k_s^B \cdot k_{CM}^B}$. Based on (Rossomme et al., 2021), the uncertainty in the product $k_s^i \cdot k_{CM}^i$ for each gap was taken as 0.3% (type-B). The type-A uncertainty in M_i, given by the standard deviation of the mean under Co-60 calibration, was 0.05%. The combined uncertainty in the air gap ratio (u_{d_R}) is obtained using gaussian error propagation of the previous variables: $u_{d_R}^2 = \left(\frac{\partial d_R}{\partial M_T}\right)^2 u_{M_T}^2 + \left(\frac{\partial d_R}{\partial M_B}\right)^2 u_{M_B}^2 + \left(\frac{\partial d_R}{\partial k_s^T \cdot k_{CM}^T}\right)^2 u_{k_s^T \cdot k_{CM}^T}^2 + \left(\frac{\partial d_R}{\partial k_s^B \cdot k_{CM}^B}\right)^2 u_{k_s^B \cdot k_{CM}^B}^2$. With this approach, $u_{d_R}$is 0.4%.

Beam quality correction factors: The uncertainties in k_{Q,Q_0}^i for each gap were estimated as 0.4%, 0.7%, and 1.6% for electrons, protons, and carbon ions, respectively. These mainly stem from the uncertainty in w_{air}. However, when taking the ratio k_{Q,Q_0}^R, the w_{air} terms cancel, reducing the relative uncertainty on the ratio of beam quality correction factors (u_{k_{Q,Q_0}^R}) to 0.6% for all particles. This value originates from a combination of type-A uncertainties over the dose values. Type-B uncertainties are also associated with MC calculations, primarily related to stopping power data, scattering data, and nuclear interaction data; however, since a ratio is calculated, these can be considered highly, if not fully, correlated.

Collected charge: The uncertainty in the collected charge M_i arises from type-A uncertainty (standard deviation of the mean) under the experimental conditions being studied. In this work, the propagated uncertainty in the charge ratio (obtained from Gaussian error propagation as:

$u_{M_R}^2 = \left(\frac{\partial M_R}{\partial M_T}\right)^2 u_{M_T}^2 + \left(\frac{\partial M_R}{\partial M_B}\right)^2 u_{M_B}^2$) was 0.07% for carbon, 0.7% for UHDR protons, and 1.5% for UHDPP electrons, reflecting the higher output instabilities of some beams, especially in UHDR and UHDPP conditions.

The total combined uncertainty in k_s is obtained by Gaussian propagation of the uncertainties from all sources, assumed to be independent from each other:

$$u_{k_s}^2 = \left(\frac{\partial k_s}{\partial V_R}\right)^2 u_{V_R}^2 + \left(\frac{\partial k_s}{\partial d_R}\right)^2 u_{d_R}^2 + \left(\frac{\partial k_s}{\partial k_{Q,Q_0}^R}\right)^2 u_{k_{Q,Q_0}^R}^2 + \left(\frac{\partial k_s}{\partial M_R}\right)^2 u_{M_R}^2$$

The largest contribution in the combined uncertainty arises from the ratio of the beam quality correction factors. As shown in Equation (6), k_{Q,Q_0}^R effectively reduces to the ratio of absorbed doses, which, for the very thin layer of material, is effectively the same. One way to reduce the associated uncertainty is to directly determine the air-gap size with the method described in the beam of interest (in which k_{Q,Q_0}^R is no longer needed). Considering the thin material layer between both air cavities and the use of the detector in conditions without significant dose gradients, a reasonable assumption is that the DGIC method is beam quality independent.

With this assumption, the overall uncertainty in k_s estimated with the DGIC method is approximately 0.62% for carbon ions, 0.85% for the UHDR proton beam, and 2.26% for the UHDPP electron beam. The main contributions on uncertainty come from the standard deviation of the ratio of collected charges, which depends on detector design and on beam output stability.

Disclosure and acknowledgements:

S. Rossomme, K. Souris, V. de Beco, T. Haas and N. Durny are employees of IBA Dosimetry. This study has been made in close collaboration with IBA Dosimetry. The double gap ionization chamber prototype was designed and built at IBA Dosimetry, with the direct involvement of Marina Orts Sanz, Victor De Beco, Thomas Haas, and Séverine Rossomme.

This work has been funded by the Walloon Region under the project name D-CAF (Dosimetry for Carbon, ARC, and FLASH therapies), MecaTech/BioWin convention #8510. The authors would like to thank all those who provided support and assistance during the measurements carried out at the various facilities.

Bibliography:

Agostinelli, S., Allison, J., Amako, K., Apostolakis, J., Araujo, H., Arce, P., Asai, M., Axen, D., Banerjee, S., Barrand, G., Behner, F., Bellagamba, L., Boudreau, J., Broglia, L., Brunengo, A., Burkhardt, H., Chauvie, S., Chuma, J., Chytracek, R., … Zschiesche, D. (2003). *Geant4—a simulation toolkit*. https://doi.org/10.1016/s0168-9002(03)01368-8

Almond, P., Biggs, P., Coursey, B., Hanson, W., Huq, M., Nath, R., & Rogers, D. (1999). AAPM's TG-51 protocol for clinical reference dosimetry of high-energy photon and electron beams. In *Medical Physics (Lancaster)*. https://doi.org/10.1118/1.598691

Andreo, P., Wulff, J., Burns, D., & Palmans, H. (2013). Consistency in reference radiotherapy dosimetry: resolution of an apparent conundrum when 60Co is the reference quality for charged-particle and photon beams. *Physics in Medicine and Biology*. https://doi.org/10.1088/0031-9155/58/19/6593

Boag J W. (1950). Ionization measurements at very high intensities. Pulsed radiation beams. *British Journal of Radiology*. https://doi.org/10.1259/0007-1285-23-274-601

Boag, J. W., & Currant, J. (1980). Current collection and ionic recombination in small cylindrical ionization chambers exposed to pulsed radiation. In *The British journal of radiology*. https://doi.org/10.1259/0007-1285-53-629-471

Boag, J. W., Hochhäuser, E., & Balk, O. A. (1996). The effect of free-electron collection on the recombination correction to ionization measurements of pulsed radiation. In *Phys. Med. Biol* (Vol. 41). http://iopscience.iop.org/0031-9155/41/5/005

Boag, J., & Wilson, T. (1952). *The saturation curve at high ionization intensity*. https://doi.org/10.1088/0508-3443/3/7/305

Bourgouin, A., Hackel, T., & Kapsch, R. (2023). The PTB water calorimeter for determining the absolute absorbed dose to water in ultra-high pulse dose rate electron beams. *Physics in Medicine and Biology*. https://doi.org/10.1088/1361-6560/acce1d

Bourgouin, A., Hackel, T., Marinelli, M., Kranzer, R., Schüller, A., & Kapsch, R. (2022). Absorbed-dose-to-water measurement using alanine in ultra-high-pulse-dose-rate electron beams. *Physics in Medicine and Biology*. https://doi.org/10.1088/1361-6560/ac950b

Bourgouin, A., Paz-Martín, J., Gedik, Y. C., Frei, F., Peier, P., Rossomme, S., Schönfeld, A. A., Schüller, A., Rodríguez, F. G., & Kapsch, R. (2023). Charge collection efficiency of commercially available parallel-plate ionisation chambers in ultra-high dose-per-pulse electron beams. *Physics in Medicine and Biology*. https://doi.org/10.1088/1361-6560/ad0a58

Bourhis, J., Montay-Gruel, P., Jorge, P. G., Bailat, C., Petit, B., Ollivier, J., Jeanneret-Sozzi, W., Ozsahin, M., Bochud, F., Moeckli, R., Germond, J.-F., & Vozenin, M.-C. (2019). Clinical translation of FLASH radiotherapy: Why and how? *Radiotherapy and Oncology*. https://doi.org/10.1016/j.radonc.2019.04.008

Christensen, J. B., Almhagen, E., Stolarczyk, L., Liszka, M., Hernandez, G. G., Bassler, N., Nørrevang, O., & Vestergaard, A. (2020). Mapping initial and general recombination in scanning proton pencil beams. *Physics in Medicine and Biology*, *65*(11). https://doi.org/10.1088/1361-6560/ab8579

Fenwick, J. D., & Kumar, S. (2022). Collection efficiencies of ionization chambers in pulsed radiation beams: an exact solution of an ion recombination model including free electron effects. *Physics in Medicine and Biology*. https://doi.org/10.1088/1361-6560/aca74e

Fleta, C., Pellegrini, G., Godignon, P., Rodríguez, F. G., Paz-Martín, J., Kranzer, R., & Schüller, A. (2024). State-of-the-art silicon carbide diode dosimeters for ultra-high dose-per-pulse radiation at FLASH radiotherapy. *Physics in Medicine and Biology*. https://doi.org/10.1088/1361-6560/ad37eb

García, L. I. R., Pérez-Azorín, J. F., Anguiano, M., & Lallena, A. M. (2021). Monte Carlo calculation of charge collection efficiencies in ionization chambers. *Physics in Medicine and Biology*. https://doi.org/10.1088/1361-6560/ABD4F8

Gómez, F., González-Castaño, D., Fernández, N. G., Pardo-Montero, J., Schüller, A., Gasparini, A., Vanreusel, V., Verellen, D., Felici, G., Kranzer, R., & Paz-Martín, J. (2022). Development of an ultra-thin parallel plate ionization chamber for dosimetry in FLASH radiotherapy. In *Medical Physics (Lancaster)*. https://doi.org/10.1002/MP.15668

Houyoux, G., Penninckx, S., Rossomme, S., Souris, K., Palmans, H., & Reynaert, N. (2025). Impact of manufacturing tolerances on Monte Carlo calculated kQQ0 factors for plane-parallel ionisation chambers in proton beams. *Physics in Medicine and Biology*. https://doi.org/10.1088/1361-6560/adc86b

INTERNATIONAL ATOMIC ENERGY AGENCY. (2024). *Absorbed Dose Determination in External Beam Radiotherapy, Technical Report Series No. 398 (Rev.1)* (Issue Technical Report Series No. 398 (Rev. 1)). INTERNATIONAL ATOMIC ENERGY AGENCY. https://doi.org/https://doi.org/10.61092/iaea.ve7q-y94k

Jaffé, G. (1913). Zur Theorie der Ionisation in Kolonnen. *Annalen Der Physik*. https://doi.org/10.1002/ANDP.19133471205

Jaffé, G. (1929). Zur Theorie der Ionisation in Kolonnen. II. *Annalen Der Physik*. https://doi.org/10.1002/ANDP.19293930706

Karsch, L., Beyreuther, E., Burris-Mog, T., Kraft, S., Richter, C., Zeil, K., & Pawelke, J. (2012). Dose rate dependence for different dosimeters and detectors: TLD, OSL, EBT films, and diamond detectors. *Medical Physics*. https://doi.org/10.1118/1.3700400

Khan, A., Simiele, E. A., & Dewerd, L. (2021). Monte Carlo-derived ionization chamber correction factors in therapeutic carbon ion beams. *Physics in Medicine and Biology*. https://doi.org/10.1088/1361-6560/ac226c

Kranzer, R., Schüller, A., Bourgouin, A., Hackel, T., Poppinga, D., Lapp, M., Looe, H., & Poppe, B. (2022). Response of diamond detectors in ultra-high dose-per-pulse electron beams for dosimetry at FLASH radiotherapy. *Physics in Medicine and Biology*. https://doi.org/10.1088/1361-6560/ac594e

Kranzer, R., Schüller, A., Rodríguez, F. G., Weidner, J., Paz-Martín, J., Looe, H., & Poppe, B. (2022). Charge collection efficiency, underlying recombination mechanisms, and the role of electrode distance of vented ionization chambers under ultra-high dose-per-pulse conditions. *Physica Medica (Testo Stampato)*. https://doi.org/10.1016/j.ejmp.2022.10.021

Liu, K., Holmes, S., Khan, A., Hooten, B. D., DeWerd, L. A., Schüler, E., & Beddar, S. (2024). Development of novel ionization chambers for reference dosimetry in electron flash radiotherapy. *Medical Physics (Lancaster)*. https://doi.org/10.1002/mp.17425

Liu, K., Velasquez, B., & Schüler, E. (2023). Technical note: High-dose and ultra-high dose rate (UHDR) evaluation of Al_2O_3:C optically stimulated luminescent dosimeter nanoDots and powdered LiF:Mg,Ti

thermoluminescent dosimeters for radiation therapy applications. *Medical Physics*. https://doi.org/10.1002/mp.16832

Lourenço, A., Subiel, A., Lee, N., Flynn, S., Cotterill, J., Shipley, D. R., Romano, F., Speth, J., Lee, E., Zhang, Y., Xiao, Z., Mascia, A., Amos, R. A., Palmans, H., Thomas, R. A. S., Lourenço, A., Subiel, A., Lee, N., Flynn, S., … Thomas, R. A. S. (2023). Absolute dosimetry for FLASH proton pencil beam scanning radiotherapy. *Scientific Reports*. https://doi.org/10.1038/s41598-023-28192-0

Martino, F. Di, Sarto, D. Del, Bisogni, M. G., Capaccioli, S., Galante, F., Gasperini, A., Linsalata, S., Mariani, G., Pacitti, M., Paiar, F., Ursino, S., Vanreusel, V., Verellen, D., & Felici, G. (2022). A new solution for UHDP and UHDR (Flash) measurements: Theory and conceptual design of ALLS chamber. *Physica Medica (Testo Stampato)*. https://doi.org/10.1016/j.ejmp.2022.08.010

Mora, G., Maio, A., & Rogers, D. W. O. (1999). Monte Carlo simulation of a typical 60Co therapy source. *Medical Physics*. https://doi.org/10.1118/1.598770

Motta, S., Bello, R. D., Christensen, J. B., Bossin, L., & Yukihara, E. (2024). Dosimetry of ultra-high dose rate electron beams using thermoluminescence and optically stimulated luminescence detectors. *Physics in Medicine and Biology*. https://doi.org/10.1088/1361-6560/ad1cf5

Okpuwe, C., Amato, A., D'Amico, I., Liso, V. De, Napoli, M. De, martino, F. di, Felici, G., Galluzzo, L., Medina, E., Vignati, A., Camarda, M., Romano, F., & Milluzzo, G. (2024). Silicon carbide detectors for dosimetry and monitoring of ultra-high dose rate beams. *Journal of Instrumentation*. https://doi.org/10.1088/1748-0221/19/03/c03064

Orts, M., Gedik, Y. C., Bourgouin, A., Kapsch, R., Koumeir, C., Sounalet, T., Rossomme, S., Souris, K., & Sterpin, E. (2025). Radiation damage evaluation of materials for radiotherapy quality assurance devices under high dose and ultra-high dose rate electron and proton beams. *Physics in Medicine and Biology*. https://doi.org/10.1088/1361-6560/adf796

Orts, M., Rossomme, S., Souris, K., & Sterpin, E. (2024). Monte Carlo simulation of initial and volume ion recombination correction factor in plane parallel ionization chambers exposed to ion beams. *Physics in Medicine and Biology*. https://doi.org/10.1088/1361-6560/ad6730

Palmans, H., Thomas, R., & Kacperek, A. (2006). Ion recombination correction in the Clatterbridge Centre of Oncology clinical proton beam. In *Physics in medicine and biology*. https://doi.org/10.1088/0031-9155/51/4/010

Paz, I. L., Fleta, C., Gómez, F., González, D., & Pellegrini, G. (2024). First use of silicon carbide detectors with graphene-enhanced contacts for medical dosimetry. *Scientific Reports*. https://doi.org/10.1038/s41598-024-56544-x

Paz-Martín, J., Schüller, A., Bourgouin, A., González-Castaño, D. M., Gómez-Fernández, N., Pardo-Montero, J., Gómez, F., Paz-Martín, J., Schüller, A., Bourgouin, A., González-Castaño, D. M., Gómez-Fernández, N., Pardo-Montero, J., & Gómez, F. (2022). *Numerical modeling of air-vented parallel plate ionization chambers for ultra-high dose rate applications*. https://doi.org/10.1016/J.EJMP.2022.10.006

Petersson, K., Jaccard, M., Germond, J., Buchillier, T., Bochud, F., Bourhis, J., Vozenin, M., & Bailat, C. (2017). High dose-per-pulse electron beam dosimetry — A model to correct for the ion recombination in the Advanced Markus ionization chamber. *Medical Physics*. https://doi.org/10.1002/MP.12111

Prieels, D. (2009). *Device and Method for Measuring an Energy Particle Beam* (Issue WO2011009953A1).

Romano, F., Milluzzo, G., Martino, F. D. Di, D'Oca, M. C., Felici, G., Galante, F., Gasparini, A., Mariani, G., Marrale, M., Medina, E., Pacitti, M., Sangregorio, E., Vanreusel, V., Verellen, D., Vignati, A., & Camarda, M. (2023). First Characterization of Novel Silicon Carbide Detectors with Ultra-High Dose Rate Electron Beams for FLASH Radiotherapy. *Applied Sciences*. https://doi.org/10.3390/app13052986

Rossomme, S., Delor, A., Lorentini, S., Vidal, M., Brons, S., Jkel, O., Cirrone, G. A. P., Vynckier, S., & Palmans, H. (2020). Three-voltage linear method to determine ion recombination in proton and light-ion beams. *Physics in Medicine and Biology*, *65*(4). https://doi.org/10.1088/1361-6560/ab3779

Rossomme, S., Hopfgartner, J., Lee, N. D., Delor, A., Thomas, R. A. S., Romano, F., Fukumura, A., Vynckier, S., & Palmans, H. (2016). Ion recombination correction in carbon ion beams. *Medical Physics*, *43*(7), 4198–4208. https://doi.org/10.1118/1.4953637

Rossomme, S., Horn, J., Brons, S., Jäkel, O., Mairani, A., Ciocca, M., Floquet, V., Romano, F., Rodriguez Garcia, D., Vynckier, S., & Palmans, H. (2017). Ion recombination correction factor in scanned light-ion beams for absolute dose measurement using plane-parallel ionisation chambers. *Physics in Medicine and Biology*, *62*(13), 5365–5382. https://doi.org/10.1088/1361-6560/aa730f

Rossomme, S., Lorentini, S., Vynckier, S., Delor, A., Vidal, M., Lourenço, A., & Palmans, H. (2021). Correction of the measured current of a small-gap plane-parallel ionization chamber in proton beams in the presence of charge multiplication. *Zeitschrift Fur Medizinische Physik*. https://doi.org/10.1016/J.ZEMEDI.2021.01.008

Schaefer, R., Psoroulas, S., & Weber, D. C. (2023). In situ correction of recombination effects in ultra-high dose rate irradiations with protons. In *Physics in Medicine and Biology*. https://doi.org/10.1088/1361-6560/ACCF5C

Stock, M., Georg, D., Ableitinger, A., Zechner, A., Utz, A., Mumot, M., Kragl, G., Hopfgartner, J., Gora, J., Bohlen, T. T., Grevillot, L., Kuess, P., Steininger, P., Deutschmann, H., & Vatnitsky, S. (2018). The technological basis for adaptive ion beam therapy at MedAustron: Status and outlook. *Zeitschrift Für Medizinische Physik*. https://doi.org/10.1016/j.zemedi.2017.09.007

Vanreusel, V., Vallet, H., Wijnen, J. P., Côté, B., Leblans, P., Sterckx, P., Vandenbroucke, D., Verellen, D., & Nascimento, L. de F. (2024). In-Vivo Dosimetry for Ultra-High Dose Rate (UHDR) Electron Beam FLASH Radiotherapy Using an Organic (Plastic), an Organic–Inorganic Hybrid and an Inorganic Point Scintillator System. *Photonics*. https://doi.org/10.3390/photonics11090865

Villoing, D., Koumeir, C., Bongrand, A., Guertin, A., Haddad, F., Métivier, V., Poirier, F., Potiron, V., Servagent, N., Supiot, S., Delpon, G., & Chiavassa, S. (2022). Proton beam dosimetry at ultra-high dose rates (FLASH): evaluation of GAFchromic™ (EBT3, EBT-XD) and OrthoChromic (OC-1) film performances. *Medical Physics (Lancaster)*. https://doi.org/10.1002/mp.15526

Vozenin, M., Loo, B. W., Tantawi, S., Maxim, P. G., Spitz, D. R., Bailat, C., & Limoli, C. (2024). FLASH: New intersection of physics, chemistry, biology, and cancer medicine. *Reviews of Modern Physics*. https://doi.org/10.1103/revmodphys.96.035002

Vozenin, M.-C., Bourhis, J., & Durante, M. (2022). Towards clinical translation of FLASH radiotherapy. *Nature Reviews Clinical Oncology*. https://doi.org/10.1038/s41571-022-00697-z

Zhou, S., Zheng, D., Fan, Q., Yan, Y., Wang, S., Lei, Y., Besemer, A. E., Zhou, C., & Enke, C. A. (2020). Minimum dose rate estimation for pulsed FLASH radiotherapy: A dimensional analysis. *Medical Physics (Lancaster)*. https://doi.org/10.1002/mp.14181